analytical chemistry

Article

pubs.acs.org/ac

Near-Infrared Silver Cluster Optically Signaling Oligonucleotide Hybridization and Assembling Two DNA Hosts

Jeffrey T. Petty,*,† David A. Nicholson, Orlin O. Sergev, and Stuart K. Graham

Department of Chemistry, Furman University, Greenville, South Carolina 29613, United States

Supporting Information

ABSTRACT: Silver clusters with ~10 atoms form within DNA strands, and the conjugates are chemical sensors. The DNA host hybridizes with short oligonucleotides, and the cluster moieties optically respond to these analytes. Our studies focus on how the cluster adducts perturb the structure of their DNA hosts. Our sensor is comprised of an oligonucleotide with two components: a 5′-cluster domain that complexes silver clusters and a 3′-recognition site that hybridizes with a target oligonucleotide. The single-stranded sensor encapsulates an ~11 silver atom cluster with violet absorption at 400 nm and with minimal emission. The recognition site hybridizes with complementary oligonucleotides, and the violet cluster converts to an emissive near-infrared cluster with absorption at 730 nm. Our key finding is that the near-infrared cluster coordinates two of its hybridized hosts. The resulting tertiary structure was investigated using intermolecular and intramolecular variants of the same dimer. The intermolecular dimer assembles in concentrated (~5 μM) DNA solutions. Strand stoichiometries and orientations were chromatographically determined using thymine-modified complements that increase the overall conjugate size. The intramolecular dimer develops within a DNA scaffold that is founded on three linked duplexes. The high local cluster concentrations and relative strand arrangements again favor the antiparallel dimer for the near-infrared cluster. When the two monomeric DNA/violet cluster conjugates transform to one dimeric DNA/near-infrared conjugate, the DNA strands accumulate silver. We propose that these correlated changes in DNA structure and silver stoichiometry underlie the violet to near-infrared cluster transformation.

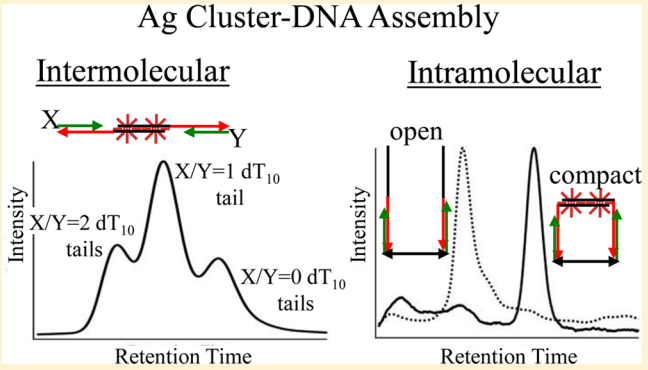

Gold and silver clusters with diameters <1 nm have ≲40 atoms.[1] Because of their small sizes, these clusters have sparsely organized electronic states and exhibit structured optical spectra, strong emission, weakly coupled states, and significant highest occupied molecular orbital−lowest unoccupied molecular orbital (HOMO−LUMO) energy gaps.[1−4] Cluster stoichiometry, structure, and oxidation state dictate the molecule-like electronic organizations of silver clusters, and specific clusters differ significantly in their optical, electronic, and catalytic properties.[5−9] Our studies utilize spectral and photophysical differences between clusters and optically identify specific oligonucleotides (Figure 1). This detection strategy uses DNA ligands to form specific cluster adducts. The electron-rich functional groups within the DNA nucleobases coordinate and stabilize surface atoms and curtail cluster growth.[10−15] Encapsulated clusters have ~10 silver atoms and form optical labels with $\varepsilon \sim 10^5$ M^{-1} cm^{-1} and $\phi_f \sim 30\%$.[16−18] Both DNA sequence and structure define binding sites for silver clusters. Different primary sequences create clusters with discrete, resolved electronic bands that span the visible and near-infrared regions.[16,17,19,20] Secondary and tertiary DNA structure also distinguish silver clusters. For example, protonation reversibly regulates the folded structure of a cytosine-rich DNA strand and its associated environment for a red-emitting silver cluster.[21]

DNA structures and cluster binding sites are also controlled by complementary strands. Oligonucleotide hosts for silver clusters are large in relation to their ~10 silver atom adducts, so they can integrate cluster binding sites and recognition sites for analytes.[22−27] Such DNA strands hybridize with oligonucleotide analytes and trigger large fluorescence changes and absorption shifts in their cluster moieties.[13−15,22,26,28,29] Their stark spectral and photophysical changes rival the responses from other sensors such as molecular beacons.[22,28,30] Furthermore, silver cluster labels are conveniently synthesized in situ using a DNA template, Ag^+, and the reducing agent BH_4^-. To understand how these silver cluster/DNA conjugates optically sense analytes, we designed a general oligonucleotide sensor with a 5′ component that complexes silver clusters and a 3′ component that hybridizes with a target oligonucleotide.[28,31] This composite single-stranded oligonucleotide exclusively forms an ~11 silver atom cluster with violet absorption and

Received: June 13, 2014
Accepted: August 26, 2014
Published: August 26, 2014

   dx.doi.org/10.1021/ac502192w | Anal. Chem. 2014, 86, 9220−9228

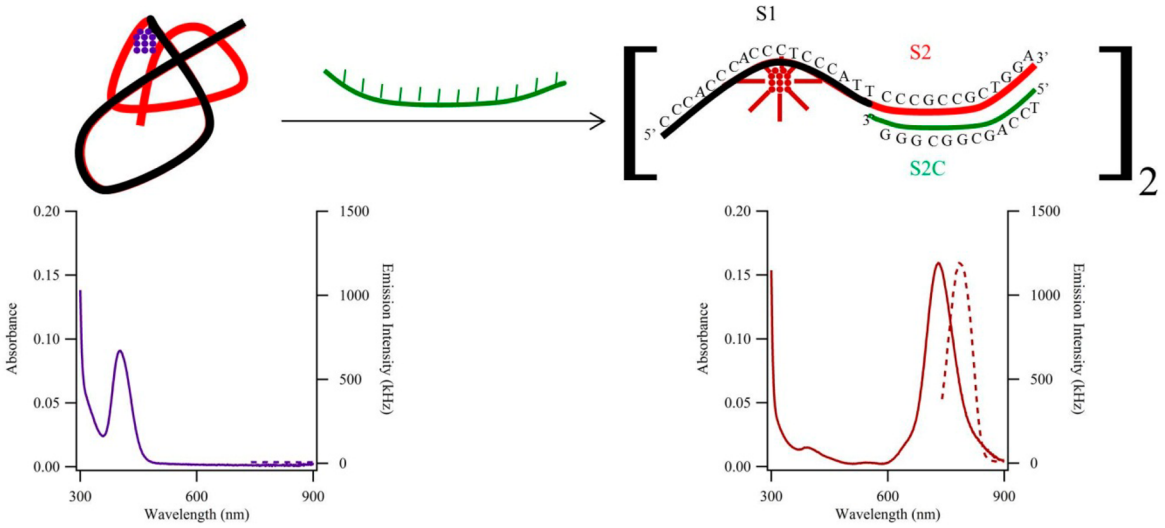

Figure 1. Reaction scheme with absorption (solid line) and emission (dotted lines) spectra associated with the S1-S2$_a$/violet cluster complex (left) and the S1-S2/S2C$_a$/near-infrared cluster complex (right).

Table 1. Oligonucleotides Used for These Studies[a]

S1-S2$_a$	CCCACCCACCCTCCCA-TT-CCCGCCGCTGGA
S2C$_a$	TCCAGCGGCGGG
S1-S2$_b$	CCCACCCACCCTCCCA-TT-CCCGGCGCGGG
S1-S2-T$_{20}$	CCCACCCACCCTCCCA-TT-CCCGGCGCGGG-TTTTTTTTTTTTTTTTTTTT
S2C$_b$	CCCGCGCCGGG
S1-S2$_c$	CCCACCCACCCTCCCA-TT-CCCGTCGACCG
X$_{11}$-S2C$_b$	GCGGCGTCCGCTT-CCCGCGCCGGG
Y$_{11}$-S2C$_b$	GCGGACGCCGCTT-CCCGCGCCGGG
X$_{21}$-S2C$_b$	GCGGCGTCCGCGGCCGTGACG-TT-CCCGCGCCGGG
Y$_{21}$-S2C$_b$	CGTCACGGCCGCGGACGCCGC-TT-CCCGCGCCGGG
Y$_{21}$-S2C$_c$	CGTCACGGCCGCGGACGCCGC-TT-CGGTCGACGGG
X$_{32}$-S2C$_b$	GCGGCGTCCGCGGCCGTGACGTGAGCGCGTGC-TT-CCCGCGCCGGG
Y$_{32}$-S2C$_b$	GCACGCGCTCACGTCACGGCCGCGGACGCCGC-TT-CCCGCGCCGGG
X$_{42}$-S2C$_b$	GCGGCGTCCGCGGCCGTGACGTGAGCGCGTGCAATCGTAGCG-TT-CCCGCGCCGGG
Y$_{42}$-S2C$_b$	CGCTACGATTGCACGCGCTCACGTCACGGCCGCGGACGCCGC-TT-CCCGCGCCGGG

[a]Strand polarity is 5′ → 3′, left → right. The sequence is formatted as follows: S1 designates the cluster domain, S2 designates the recognition site, S2C is the complementary strand for the recognition site, X and Y are the duplex components. For the latter sequences, the subscripts designate the number of nucleotides in the strand. Oligonucleotides were received from Integrated DNA Technologies as lyophilized and desalted samples and were used without further purification. The oligonucleotides were dissolved in water, and their concentrations were measured using the absorbance at 260 nm based on extinction coefficients derived from the nearest-neighbor approximation. Concentrations were measured in a 10 mM boric acid/borate buffer with pH = 9.8, which disrupts aggregates favored by cytosine-rich strands.[58,59] Duplexes were annealed by heating equimolar amounts of single strands together to 95 °C for 5 min with slow cooling to room temperature for >5 h.

minimal emission. The resulting DNA/cluster conjugate hybridizes with the target complementary strand and adopts a mixed single-/double-stranded secondary structure. In concert with this structural change, the violet cluster converts to a near-infrared cluster with a >300 nm shift in absorption and an ∼60-fold emission enhancement (Figure 1). The spectra of this latter cluster lie within the optical window where scattering, absorption, and endogenous emission from biological samples are minimized.[32] Thus, this bright, high-contrast fluorophore is a promising label and reporter for vivo sensing and imaging.[33,34]

Our studies establish a link between optical switching by the cluster moieties and aggregation by the DNA hosts. Two variants explore this noncanonical DNA assembly. An intermolecular DNA aggregate was identified by appending thymines on the target complementary strand and increasing the overall conjugate size. A mixture of normal and thymine-tagged complements generates three near-infrared conjugates, and their chromatographic distribution reveals a dimeric DNA host with antiparallel strand orientations. The conjugate stoichiometry, structure, and stability suggest that the DNA dimerizes because the near-infrared cluster coordinates two of its DNA hosts. An intramolecular variant of this same DNA dimer develops within a larger DNA scaffold. This scaffold expands the scope of DNA ligands for silver clusters because hybridization directs the cluster transformation. The scaffold is founded on a mediating duplex that cohybridizes with two DNA/violet cluster conjugates. The composite ligand locally concentrates the two violet clusters and facilitates transformation to the near-infrared cluster. The resulting near-infrared cluster/DNA conjugate substantiates the stoichiometry and structure of its intermolecular analogue. Furthermore, the scaffold constrains the cluster environment through the length of its mediating duplex. These allosteric changes support

dx.doi.org/10.1021/ac502192w | Anal. Chem. 2014, 86, 9220−9228

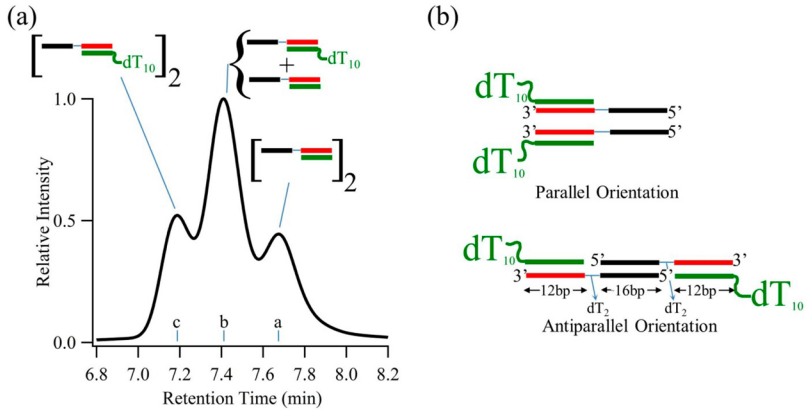

Figure 2. (a) Equimolar amounts of $S2C_a$ and dT_{10}-$S2C_a$ yielded three near-infrared conjugates with different numbers of protruding thymines. (b) Two models for the parallel and antiparallel orientations of the two S1-$S2_a$/$S2C_a$ strands.

substantial overlap of the encapsulating strands in the dimer. The dimeric DNA host also amasses silver atoms from its two monomeric DNA/violet cluster precursors. Our studies evaluate this relationship between DNA structure, silver stoichiometry, and optical switching from the violet to near-infrared clusters.

EXPERIMENTAL SECTION

Our synthetic protocol and characterization followed earlier studies.[28] The oligonucleotides used for these studies are listed in Table 1. The precursor violet cluster-DNA conjugate was formed by mixing 90 μM solution of the oligonucleotide S1-S2 with 8 equiv of Ag^+/oligonucleotide in a 10 mM citrate/citric acid buffer at pH = 6.5 with $[Na^+] \approx 26$ mM.[35] The Ag^+ was reduced with 4 equiv of BH_4^-/oligonucleotide.[27] This solution was exposed to 500 psi O_2 at room temperature for >3 h to favor the precursor violet cluster. Complementary strands form the near-infrared cluster in solutions with 300 mM Na^+. Absorption spectra were acquired with a Cary 50 (Varian), and emission spectra were acquired with a FluoroMax-3 (Jobin Yvon). Size exclusion chromatography was conducted with a Shimadzu Prominence high-performance liquid chromatography system using a 300 mm × 7.8 mm BioSep-SEC-S2000 column (Phenomenex), having 5 μm particles and a pore size of 145 Å. The mobile phase was buffered at pH = 6.5 with 10 mM citrate/citric acid that was supplemented with $NaClO_4$ to minimize solute interactions with the stationary phase.[36] To assess hydrodynamic radii, size standards were based on the thymine oligonucleotides dT_{10}, dT_{15}, dT_{20}, and dT_{30}.[21,37]

RESULTS

A silver cluster with near-infrared absorption and emission develops a higher-order DNA structure. Below, we describe the spectral development of this cluster and the structural transformation of its DNA host.

DNA Structure Dictates Cluster Environments. Our studies are based on the core oligonucleotide S1-S2. Its two components dictate the secondary structures and cluster environments of this strand (Figure 1).[28] The 5′-S1 sequence CCCACCCACCCTCCCA (black) was chosen because this sequence favors near-infrared silver clusters.[38] This cluster domain was linked via dT_2 to the 3′-S2 recognition site (red). This component binds a complementary strand S2C (green), and we chose to detect single-stranded DNA because this analyte forms strong, specific complexes with the complementary recognition site. In this and earlier studies, the sequence and length of S2 and S2C were varied to demonstrate modular DNA detection, and we first describe studies with the sequences $S2_a$ and $S2C_a$ (Table 1).[27,31] The key to our detection strategy is that the composite S1-S2 exclusively forms an ~11 silver atom cluster with λ_{max} = 400 nm (solid line) and with minimal emission (dotted line) (Figure 1, left). DNA strands can produce a range of clusters, but this violet species emerges over alternate clusters by using relatively low Ag^+/DNA concentrations, low ionic strength buffers, and high O_2 concentrations.[27,38,39]

Our studies focus on the successor to this cluster. The single-stranded S1-$S2_a$/violet cluster conjugate hybridizes with its complement $S2C_a$, and the resulting S1-$S2_a$/$S2C_a$ now favors a strongly emissive cluster with $\lambda_{ex,max}$ = 730 nm (solid line) and $\lambda_{em,max}$ = 800 nm (dotted line) (Figure 1, right). Hybridization recovers the near-infrared cluster that is favored by the S1 sequence alone, and this cluster transformation optically signals the target oligonucleotide.[40] We explored the reasons for the cluster conversion by measuring the DNA stoichiometry and structure of the DNA/near-infrared cluster complex.

Cluster Promotes DNA Assembly. We first summarize our prior studies that showed DNA stoichiometry distinguishes the near-infrared cluster/DNA conjugate from its native S1-$S2_a$/$S2C_a$ host.[28] Two variants, $S2C_a$ and dT_{10}-$S2C_a$, used the same complementary sequence for $S2_a$ (Table 1). On the latter complement, the thymine appendage is chemically innocuous because it projects away from the S1 cluster domain and because neutral pH protonates and blocks the N3 cluster binding site on thymine.[28,41] Individually, $S2C_a$ and dT_{10}-$S2C_a$ hybridize with the S1-$S2_a$/violet cluster conjugate and produce single conjugates with different sizes. However, their equal mixture produces a third intermediate species (Figure 2a). The resulting temporal and intensity distribution enumerates the $S2C_a$ constituents and the S1-$S2_a$/$S2C_a$ stoichiometry. Retention times in size exclusion chromatography depend on hydrodynamic radius, and this trend is supported by the later (peak a) and earlier (peak c) elution of near-infrared cluster conjugates with the smaller $S2C_a$ and the larger dT_{10}-$S2C_a$, respectively. The intermediate retention time (peak b) suggests that this species has a mixture of both complements. In addition, this species has an ~2-fold higher intensity than its neighboring peaks, and this pattern suggests that two equivalent $S2_a$ recognition sites statistically favor both the $S2C_a$ and dT_{10}-$S2C_a$ complements. Thus, the triplet chromatographic pattern

dx.doi.org/10.1021/ac502192w | Anal. Chem. 2014, 86, 9220−9228

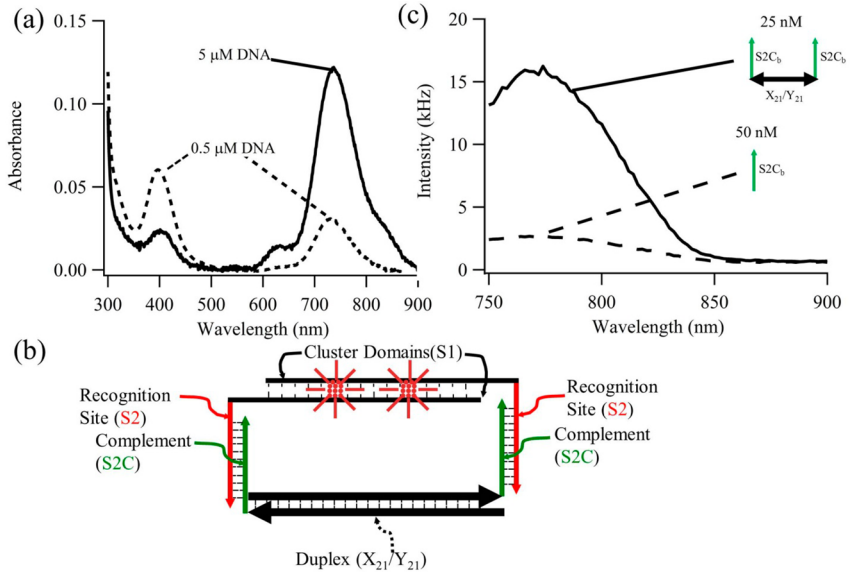

Figure 3. (a) Absorption spectra of samples with 5 (solid line) and 0.5 (dashed line) μM S1-S2$_b$/violet cluster conjugates and S2C$_b$. (b) Model for constituents in the DNA scaffold. (c) Fluorescence spectra for samples with 25 nM S2C$_b$-X$_{21}$/Y$_{21}$-S2C$_b$ (solid line) and 50 nM S2C$_b$ (dashed line) with 50 nM S1-S2$_b$/violet cluster conjugate.

supports a dimeric (S1-S2/S2C)$_2$ host for the near-infrared cluster. This DNA stoichiometry was substantiated by two other measurements.[28] The extinction coefficients of the DNA and cluster chromophores were measured using absorption and fluorescence correlation spectroscopies, and their ratio also supports a 1:2 cluster/S1-S2$_a$/S2C$_a$ stoichiometry. Fluorescence anisotropy showed that the aggregated cluster conjugate is larger than its native S1-S2$_a$/S2C$_a$ host.

Our new studies use the triplet chromatographic pattern and evaluate S1-S2$_a$ orientations within the dimer. The three near-infrared clusters have 0, 1, and 2 protruding dT$_{10}$ appendages, which alter conjugate retention times and sizes (Figure 2a, peaks a, b, and c, respectively). The relative arrangement of these appendages dictates the temporal splitting between the peaks, which we interpret using two models (Figure 2b). With a parallel S1-S2 arrangement, the thymine appendages are adjacent. The resulting size changes are expected to be smaller from 1 → 2 vs 0 → 1 appendages, so the chromatographic pattern would be asymmetric. With an antiparallel S1-S2 arrangement, the thymines project from opposing ends of the dimer. The size changes from 0 → 1 and 1 → 2 appendages are expected to be similar, thus the chromatographic pattern would be more symmetric. The temporal splittings were related to size shifts by using the logarithmic relationship between retention time and hydrodynamic radius (Supporting Information).[42] On the basis of the dimer with no appendages (peak a, Figure 2a), the size changes due to one (peak b) and two appendages (peak c) are designated α and β, respectively. A relative change β/α = 1.94 ± 0.08 suggests that the appendages contribute equally to the size changes and supports their opposing arrangement. Thus, temporal splitting pattern supports antiparallel orientations for the two S1-S2$_a$/S2C$_a$ strands that host the near-infrared cluster.

The antiparallel model suggests that the overall complex has an elongated shape. We used two experiments to investigate its global structure. First, dT$_{20}$ replaced the smaller dT$_{10}$ appendage on S2C$_a$ (Figure S1 in the Supporting Information). As with the above dT$_{10}$ studies, S2C$_a$ and dT$_{20}$-S2C$_a$ also produce a triplet chromatographic pattern but with improved resolution. The dimers that form with dT$_{20}$-S2C$_a$ further substantiate the antiparallel over the parallel model because we expect bulky substituents to favor opposing ends of the dimer. The (S1-S2$_a$/S2C$_a$)$_2$ dimers with two vs one dT$_{20}$ appendages have a relative size change β/α = 1.90 ± 0.04, which is comparable to the value with the dT$_{10}$ tags. This ~2-fold size increment suggests that both dT$_{20}$ appendages contribute equally to the overall size changes and lengthen the dimer along a major, rodlike axis. Second, DNA duplexes with 11, 20, and 40 base pairs provide a structural basis to interpret the dimer shape (Figure S2 in the Supporting Information). Short, B-form DNA duplexes form stiff polymers, and their lengths systematically shift chromatographic retention times.[43] These calibration standards show that the near-infrared cluster/DNA conjugate has a length comparable to a ~38 base pair duplex. On the basis of its primary sequence, the antiparallel dimer has a similar length of 44 nucleotides: two terminal 12 base pair duplexes and dT$_2$ linkers flank two overlapped 16 nucleotide S1 cluster domains (Figure 2b). This length comparison does not consider the flexibility and strand overlap in the dimer, which are addressed later in the paper.

Intermolecular vs Intramolecular Assembly. DNA concentration controls the violet to near-infrared cluster transformation, and we studied two samples with 5 and 0.5 μM concentrations of the S1-S2$_b$/violet conjugate and complement S2C$_b$ (Figure 3a). Their spectra compensate for the concentration differences by using pathlengths of 1 and 10 cm, respectively. The spectra show that the more dilute solution retained stronger violet absorption and yielded lower near-infrared absorption. These correlated changes support an intermolecular (S1-S2/S2C)$_2$ complex because lower concentrations inhibit its assembly via two monomeric S1-S2/violet cluster complexes.

While this DNA dimer innately forms in more concentrated solutions, it also develops within the confines of a larger DNA construct (Figure 3b). This alternative synthetic strategy parallels the intermolecular DNA reaction: S1-S2$_b$/violet cluster conjugates hybridize with complementary S2C$_b$ strands and form the near-infrared cluster. The new approach chemically

dx.doi.org/10.1021/ac502192w | Anal. Chem. 2014, 86, 9220−9228

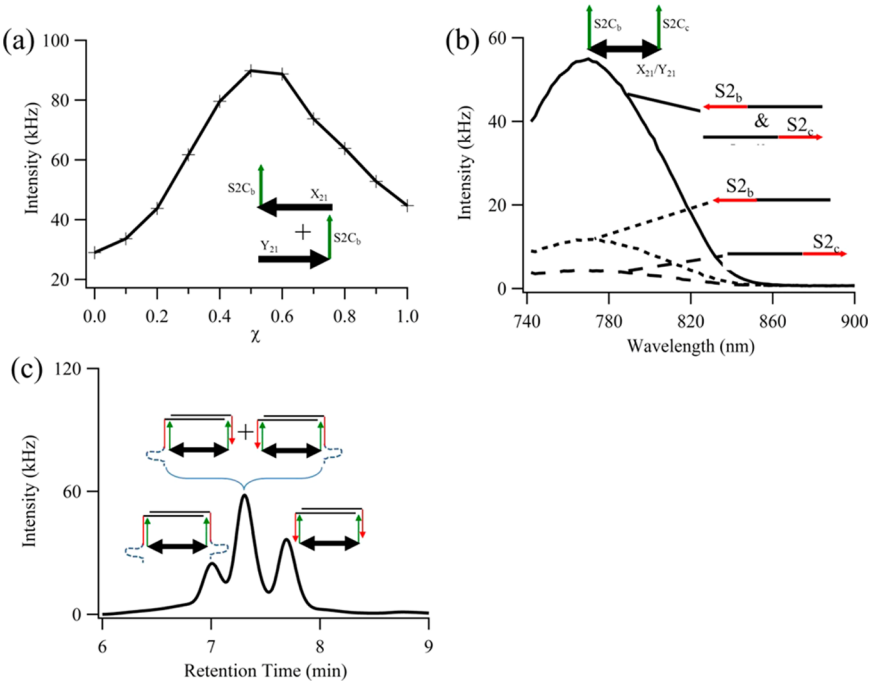

Figure 4. (a) Continuous variation analysis used solutions with fixed 100 nM concentrations of S1-$S2_b$/violet cluster conjugates and varying relative amounts of X_{21}-$S2C_b$ and Y_{21}-$S2C_b$. (b) Fluorescence spectra collected with X_{21}/Y_{21} appended with two different complementary strands $S2C_b$ and $S2C_c$. (c) Size exclusion chromatogram following the reaction of violet conjugates with S1-$S2_b$ and S1-$S2_b$-dT_{20} (dashed, blue appendage) with $S2C_b$-X_{21}/Y_{21}-$S2C_b$.

links the $S2C_b$ strands (Figure 3b). The overall construct assembles via three hybridizations. The complementary strands X_{21}-$S2C_b$ and Y_{21}-$S2C_b$ hybridize via their 21-nucleotide X_{21} and Y_{21} components (heavy black lines). The resulting duplex $S2C_b$-X_{21}/Y_{21}-$S2C_b$ has protruding $S2C_b$ appendages (green lines), which cohybridize with two S1-$S2_b$/violet cluster conjugates (black and red lines, respectively). The 21-base pair duplex X_{21}/Y_{21} separates the violet clusters by ∼7 nm and imposes an ∼18 mM local concentration, and such high concentrations should favor the near-infrared cluster (Figure 3a). Intermolecular vs intramolecular dimerization were distinguished using two solutions with identical net concentrations of $S2C_b$: a 25 nM solution of the linked $S2C_b$ strands (solid line) and a 50 nM solution of $S2C_b$ alone (dashed line) (Figure 3c). These solutions also contained 50 nM S1-$S2_b$/violet cluster. The independent complement $S2C_b$ produces relatively low emission, which is expected because this solution was 10-fold more dilute than the 0.5 μM solution used in Figure 3a. Thus, even lower DNA concentrations should further constrain intermolecular dimerization and near-infrared cluster development. In contrast, the linked $S2C_b$ strands produce strong near-infrared emission. The contrasting emission intensities suggest that the DNA construct concentrates S1−$S2_b$/violet cluster conjugates and promotes intramolecular near-infrared cluster formation. This DNA-directed cluster transformation was further interrogated by identifying the scaffold constituents that support the near-infrared cluster.

DNA Scaffold: Components and Structure. While the DNA scaffold is expected to assemble through hybridization, we also mapped its three major constituents using the near-infrared cluster emission (Figure 4). First, the relative amounts of the duplex components X_{21} and Y_{21} were determined by continuous variation analysis (Figure 4a).[44,45] Mole fractions (χ) of X_{21}-$S2C_b$ and Y_{21}-$S2C_b$ were varied, while the net concentrations of the S1-$S2_b$/violet cluster conjugates and their complementary $S2C_b$ sequences were maintained at constant 100 nM concentrations. The relative amount $\chi = 0.55 \pm 0.08$ yields the strongest near-infrared emission. This optimal ∼1:1 X_{21}-$S2C_b$/Y_{21}-$S2C_b$ stoichiometry indicates that the complementary X_{21} and Y_{21} sequences hybridize and form a duplex within the composite DNA structure. Second, two S2C components were identified by using different sequences (Figure 4b). $S2C_b$ and $S2C_c$ were designed to exclusively hybridize with S1-$S2_b$/ and S1-$S2_c$/violet cluster complexes, respectively (Table 1). The core duplex $S2C_b$-X_{21}/Y_{21}-$S2C_c$ produces low emission with either S1-$S2_b$ (dotted line) or S1-$S2_c$ (dashed line) alone but strong emission with their mixture (solid line). This favorable heterogeneous combination indicates that two S2C/S2 duplexes emanate from the X_{21}/Y_{21} duplex. Third, the S1-S2 components were enumerated with a 3′-dT_{20} appendage (Figure 4c). This approach parallels our earlier studies of the intermolecular dimer because the thymine tag enlarges the overall conjugate and distinguishes DNA dimers (Figure 2). S1-$S2_b$-dT_{20} and S1-$S2_b$ form violet cluster conjugates, and these hybridize with $S2C_b$-X_{21}/Y_{21}-$S2C_b$. Three near-infrared conjugates result. The fastest and slowest species incorporate only S1-$S2_b$-dT_{20} or S1-$S2_b$, respectively (Figure S3a in the Supporting Information). The intermediate species exhibits two key characteristics: it elutes between and produces higher emission than the flanking homogeneous analogues. These characteristics suggest that the intermediate species is statistically favored because it incorporates both S1-$S2_b$-dT_{20} and S1-$S2_b$. The intensity distribution favors the larger conjugate when the relative amount of S1-$S2_b$-dT_{20}/S1−$S2_b$ is increased from 1:1 to 1.5:1 (Figure S3b in the Supporting Information). This shift suggests that bulky thymine appendages inhibit scaffold assembly. Thus, the triplet pattern indicates that the scaffold incorporates the

dx.doi.org/10.1021/ac502192w | Anal. Chem. 2014, 86, 9220−9228

two S1-S2 strands that coordinate the near-infrared cluster. To summarize, these three experiments support a composite DNA ligand that consists of an X/Y duplex with two terminal S2/S2C duplexes. This construct uses sequence-specific hybridization and directs the dimerization of two S1 hosts for the near-infrared cluster.

The DNA scaffold also directs S1-S2 orientations within the dimer. These orientations are reflected in the shapes of the native and cluster forms of the scaffold. The native form (dotted line, Figure 5) elutes earlier than $S2C_b$-X_{21}/Y_{21}-$S2C_b$ alone (dashed line) because it acquires S1-$S2_b$/$S2C_b$ appendages. The cluster form of this composite DNA (solid line) elutes later than the corresponding native form. Its compact structure suggests that the near-infrared cluster retracts the two S1 appendages from the two ends of the X_{21}/Y_{21} duplex and forms a S1-S1 dimer with antiparallel orientations. In summary, both the intermolecular and intramolecular synthetic routes produce the same near-infrared cluster that is encapsulated by two S1strands with antiparallel orientations.

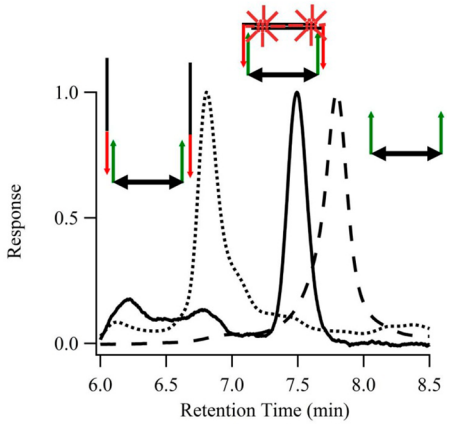

Figure 5. Size exclusion chromatograms of native $S2C_b$-X_{21}/Y_{21}-$S2C_b$, S1-$S2_b$/$S2C_b$-X_{21}/Y_{21}-$S2C_b$/$S2_b$-S1, and the cluster variant of this latter DNA construct.

DNA Scaffold: Allosteric Control. The DNA scaffold facilitates the cluster transformation by hybridizing with and concentrating two violet cluster conjugates. Furthermore, the scaffold also manipulates the cluster conversion through its structure, and we examined how the length of the X/Y duplex remotely alters overlap between the encapsulating strands (Figure 6). Duplexes with 11, 21, 32, and 42 base pairs form rigid spacers and systematically separate their S2C appendages.[43] These duplex lengths preserve the relative phases of the hybridized S1-S2 appendages.[46,47] The four $S2C_b$-X/Y-$S2C_b$ constructs produce two types of near-infrared cluster conjugates. Larger species (marked with open circles) elute earlier, and their intensities diminish with heating. These characteristics suggest that the near-infrared clusters bind to higher-order, intermolecular aggregates. Our studies focus on the more compact species (marked with stars) that elute later and are robust with heating. These characteristics suggest that one $S2C_b$-X/Y-$S2C_b$ duplex and two S1-$S2_b$/violet cluster conjugates form one composite ligand for the near-infrared cluster (Figure 3b). These intramolecular conjugates have retention times that progressively decrease from 7.85 to 7.15 min as the duplex length increases from 11 to 42 base pairs. This trend suggests that the overall size of the DNA/cluster conjugate tracks the X/Y duplex length. The duplexes also control cluster emission, and the 21-base pair duplex produces the highest emission. This duplex has a similar length to the 16

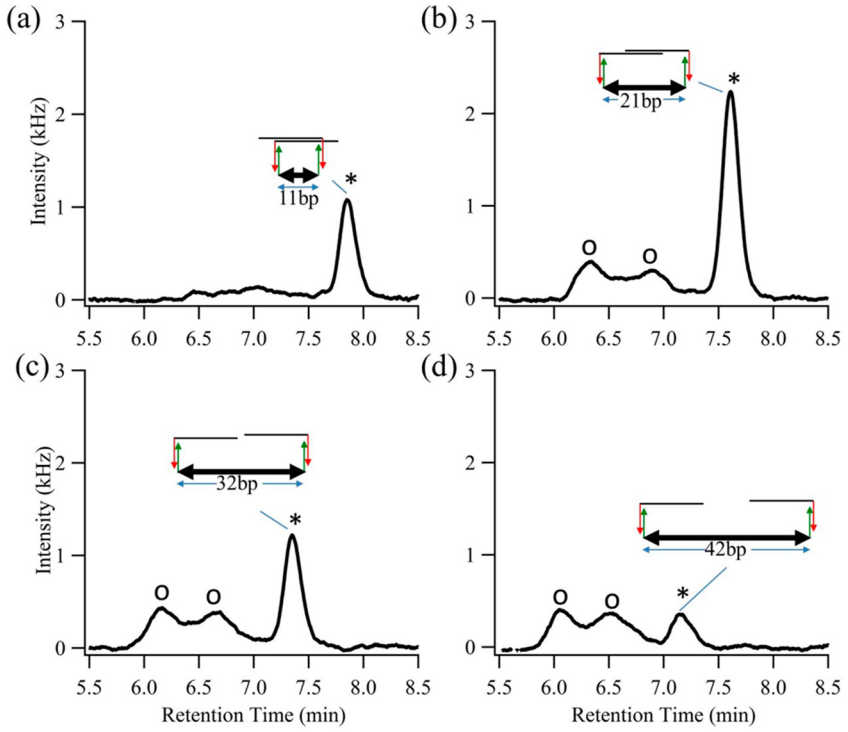

Figure 6. Size exclusion chromatograms following the reaction of violet conjugates with S1-$S2_b$ with four progressively longer duplex constructs: (a) $S2C_b$-X_{11}/Y_{11}-$S2C_b$, (b) $S2C_b$-X_{21}/Y_{21}-$S2C_b$, (c) $S2C_b$-X_{32}/Y_{32}-$S2C_b$, and (d) $S2C_b$-X_{42}/Y_{42}-$S2C_b$.

dx.doi.org/10.1021/ac502192w | Anal. Chem. 2014, 86, 9220−9228

nucleotide S1 cluster domain, and strong emission supports substantial S1-S1 overlap within the dimer.

DISCUSSION

Our studies address how silver cluster-DNA conjugates identify analytes, and the sensor strand S1-S2 serves two purposes. It hybridizes with the target analyte S2C and hosts two silver clusters with distinct optical signatures. The precursor single-stranded S1-S2 encapsulates a violet cluster, while its analyte complex S1-S2/S2C exclusively hosts an emissive near-infrared cluster (Figure 1). Our key observation is that the near-infrared cluster not only signals analyte-sensor association but also coordinates two of its DNA host strands. To demonstrate the scope of the structural transformation, we review our prior studies of the violet cluster complex with S1-S2.[27,31] This cluster has a stoichiometry of ∼11 Ag/S1-S2 and forms a monomeric complex with S1-S2. Although it is small in relation to its 30 nucleotide hosts, this cluster alters DNA structure and stability. It contracts the hydrodynamic radii of native S1-S2 strands by ∼40%.[28] It also thermodynamically stabilizes single-stranded S1-S2 and inhibits S2/S2C hybridization.[31] Both effects suggest that the violet cluster contracts and stabilizes its single-stranded DNA host because it coordinates multiple nucleobases. These results indicate that S1-S2 is a multidentate ligand, and this class of ligand finely regulates cluster environments through the positions of their coordinating groups.[48,49] We are now altering the sequence of coordinating nucleobases within S1-S2 to analogously modulate the binding site for the violet cluster.

Our new studies show that the near-infrared cluster also forms multidentate complexes with DNA. In contrast to the violet cluster that forms a monomeric intrastrand complex, the near-infrared cluster assembles two strands and yields an interstrand $(S1\text{-}S2/S2C)_2$ dimer. Our studies established its DNA stoichiometry and structure (Figure 2). The stoichiometry was deduced because the aggregate independently binds two S2C complements, and the tertiary structure was determined because the two complements bind on opposite ends of the dimer. This strand arrangement juxtaposes two single-stranded S1 sequences, which suggests that an S1-S1 dimer anchors the overall DNA structure. These native $C_3AC_3AC_3TC_3A$ sequences do not inherently self-associate, even when confined within a DNA scaffold (Figure 5). Furthermore, the cytosine-rich strands disfavor base pairing in basic solutions, yet the near-infrared cluster/$(S1\text{-}S2/S2C)_2$ complex still forms up to pH = 10.[50,18] This stability suggests that the near-infrared cluster assembles the two S1 strands. This cluster favors the single-stranded S1 sequence because it has a high proportion of cytosine, whose N3 preferentially coordinates silver clusters.[19,38,40,51,52] Theoretical calculations show that multiple cytosines preferentially stabilize small silver clusters.[52] On the basis of these observations, we suggest that the near-infrared cluster complexes with the S1 cluster domain and complexes with the cytosines in two S1 cluster domains. Intermolecular association via silver clusters may be a common structural trait because mass spectrometry studies have identified other dimeric oligonucleotide complexes with silver clusters.[39] This technique favors gas-phase aggregates because droplet desolvation produces high DNA/cluster concentrations. Our studies demonstrate that the near-infrared cluster-DNA aggregate forms in dilute aqueous solutions with nanomolar DNA concentrations (Figure 3). We are particularly interested in the stability of such aggregates because they may depend on the reaction conditions. For example, a near-infrared cluster forms a 1:1 cluster/DNA complex with the isolated S1 sequence.[38] This conjugate was studied using nonpolar solvents, so we are currently investigating the cluster/$(S1\text{-}S2/S2C)_2$ complex using different solvents.

DNA assembly via the near-infrared silver cluster is hindered in dilute solutions, but hybridization facilitates the cluster transformation under these challenging reaction conditions (Figure 3c). Two S1-S2 strands hybridize with two S2C complements on the duplex S2C-X_{21}/Y_{21}-S2C. The resulting DNA framework concentrates their violet cluster adducts and forms the near-infrared cluster. This scaffold preserves the dimeric stoichiometry and the antiparallel orientations of the S1-S2 strands that are also found in the intermolecular near-infrared cluster analogue (Figure 3b). Beyond facilitating the cluster transformation, the scaffold allosterically alters the cluster environment. We studied how remote variations in the X/Y duplex length adjust the near-infrared cluster environment (Figure 6). Four intervening duplexes rigidly separate their S1-S2/violet cluster appendages and modulate the resulting near-infrared cluster emission. Prominent emission from the 21-base pair duplex reflects a preferred cluster binding site. We propose that this environment develops because the X_{21}/Y_{21} duplex has a length that allows optimal overlap of its 16 nucleotide S1 sequences. We are now studying finer variations in the X/Y duplex lengths to adjust S1-S1 overlap in the dimer.

The scaffold for the cluster transformation shares several characteristics with DNA templates for organic reactions.[53,54] Both constructs use sequence-specific hybridization to stringently control chemical transformations, produce high local reactant concentrations that promote the reactions, require no exogenous reagents for signal transduction, and yield high contrast signals against inherently low backgrounds. The silver cluster transformations are distinct because the DNA strands are integral reaction components. Thus, the scaffold structure can dictate the positions of the S1 cluster domains and thereby modulate cluster reactivity. We showed that the X/Y duplex length allosterically modulates the near-infrared cluster environment. We are now investigating the junctions within the DNA framework. In this paper, single-stranded dT_2 junctions connected the X/Y duplex, the S2/S2C duplexes, and the S1 cluster domains. These flexible junctions promote DNA folding, but rigid four- and three-way junctions could more carefully control S1-S1 overlap in the dimer.[47,55] We are particularly interested in the relationship between the strand overlap and the electronic environment for the cluster.[19]

The DNA structural changes provide a foundation to understand optical switching by the cluster moieties. The near-infrared cluster assembles two S1-S2/S2C strands via two violet cluster complexes with S1-S2. The overall silver stoichiometry is conserved because each monomeric S1-S2/violet cluster complex has ∼11 Ag while the dimeric $(S1\text{-}S2/S2C)_2$/near-infrared cluster successor has ∼22 Ag.[28] Silver clusters in this size range have sparsely organized electronic states, and their electronic spectra depend on cluster stoichiometry and shape.[5,56,57] We propose that the correlated DNA dimerization and the silver agglomeration underlie the violet to near-infrared optical switching. We are using three models to understand organization and electronic structure of the near-infrared cluster: the two original clusters could remain chemically intact but electronically coupled, they could linearly reorganize along the DNA strand, or the two clusters could agglomerate into a larger cluster.[18,20,28] The first two cases

dx.doi.org/10.1021/ac502192w | Anal. Chem. 2014, 86, 9220−9228

suggest strong nucleobase−silver interactions, while the latter case implies strong silver−silver interactions. We are addressing these possibilities by identifying cluster binding sites within the S1-S1 dimer.

CONCLUSION

Silver clusters are encapsulated by DNA strands and form optical reporters for oligonucleotide analytes. We studied DNA reorganization that accompanies analyte recognition and the concerted cluster transformation. A single-stranded oligonucleotide coalesces around an ∼11 silver atom cluster. Complementary DNA strands hybridize with this precursor sensor and transform the violet cluster with weak emission to a near-infrared cluster with strong emission. Intermolecular and intramolecular variants show that the near-infrared cluster coordinates two DNA strands with antiparallel orientations. In conjunction with the strand dimerization, the net silver stoichiometry doubles. Understanding this relationship between silver stoichiometry and DNA organization will advance development of DNA-bound silver cluster chromophores.

ASSOCIATED CONTENT

Supporting Information

Three figures describing size exclusion chromatograms with $S2C_a$ and dT_{20}-$S2C_a$, the linear calibration of duplex strands, size exclusion chromatograms with S1-S2-dT_{20} and S1-S2/violet cluster conjugates, and the derivation of the β/α parameter that evaluates DNA shape changes. This material is available free of charge via the Internet at http://pubs.acs.org.

AUTHOR INFORMATION

Corresponding Author

*E-mail: jeff.petty@furman.edu. Phone: 864-294-2689.

Author Contributions

The manuscript was written through contributions of all authors. All authors have given approval to the final version of the manuscript.

Notes

The authors declare no competing financial interest.

†J.T.P is the Henry Keith and Ellen Hard Townes Professor of Chemistry.

ACKNOWLEDGMENTS

We thank the National Institutes of Health (Grant R15GM102818-01A1), National Science Foundation (Grant CBET-0853692), and the Arnold and Mabel Beckman Foundation. We are grateful to and National Science Foundation (Grant CHE-0922834) and the Henry Dreyfus Teacher-Scholar Awards Program for primary support during the initial stages of this work. In addition, we thank the National Science Foundation (Grants CHE-0718588 and CHE-0922834). D.A.N. and O.O.S. were supported by undergraduate research fellowships provided through the Furman Advantage program and a USE Award to Furman University from the Howard Hughes Medical Institute, respectively. J.T.P. is grateful for the support provided by the Henry Keith and Ellen Hard Townes Professorship.

REFERENCES

(1) Jin, R.; Qian, H.; Wu, Z.; Zhu, Y.; Zhu, M.; Mohanty, A.; Garg, N. *J. Phys. Chem. Lett.* **2010**, *1*, 2903−2910.
(2) Parker, J. F.; Fields-Zinna, C. A.; Murray, R. W. *Acc. Chem. Res.* **2010**, *43*, 1289−1296.
(3) Henglein, A.; Mulvaney, P.; Linnert, T. *Faraday Discuss.* **1991**, 31−44.
(4) Patel, S. A.; Cozzuol, M.; Hales, J. M.; Richards, C. I.; Sartin, M.; Hsiang, J.-C.; Vosch, T.; Perry, J. W.; Dickson, R. M. *J. Phys. Chem. C* **2009**, *113*, 20264−20270.
(5) Bonacic-Koutecky, V.; Veyret, V.; Mitric, R. *J. Chem. Phys.* **2001**, *115*, 10450−10460.
(6) Schmidt, M.; Cahuzac, P.; Bréchignac, C.; Cheng, H.-P. *J. Chem. Phys.* **2003**, *118*, 10956.
(7) Yu, J.; Patel, S. A.; Dickson, R. M. *Angew. Chem., Int. Ed.* **2007**, *46*, 1927−2121.
(8) Qian, H.; Jiang, D.-e.; Li, G.; Gayathri, C.; Das, A.; Gil, R. R.; Jin, R. *J. Am. Chem. Soc.* **2012**, *134*, 16159−16162.
(9) Li, G.; Jin, R. *Acc. Chem. Res.* **2013**, *46*, 1749−1758.
(10) Jin, R. *Nanoscale* **2010**, *2*, 343−362.
(11) Wan, X. K.; Lin, Z. W.; Wang, Q. M. *J. Am. Chem. Soc.* **2012**, *134*, 14750−14752.
(12) Pettibone, J. M.; Hudgens, J. W. *Small* **2012**, *8*, 715−725.
(13) Han, B. Y.; Wang, E. K. *Anal. Bioanal. Chem.* **2012**, *402*, 129−138.
(14) Obliosca, J. M.; Liu, C.; Batson, R. A.; Babin, M. C.; Werner, J. H.; Yeh, H.-C. *Biosensors* **2013**, *3*, 185−200.
(15) Petty, J. T.; Story, S. P.; Hsiang, J. C.; Dickson, R. M. *J. Phys. Chem. Lett.* **2013**, *4*, 1148−1155.
(16) Richards, C. I.; Choi, S.; Hsiang, J.-C.; Antoku, Y.; Vosch, T.; Bongiorno, A.; Tzeng, Y.-L.; Dickson, R. M. *J. Am. Chem. Soc.* **2008**, *130*, 5038−5039.
(17) Sharma, J.; Yeh, H. C.; Yoo, H.; Werner, J. H.; Martinez, J. S. *Chem. Commun.* **2010**, *46*, 3280−3282.
(18) Schultz, D.; Gardner, K.; Oemrawsingh, S. S. R.; Markešević, N.; Olsson, K.; Debord, M.; Bouwmeester, D.; Gwinn, E. *Adv. Mater.* **2013**, *25*, 2797−2803.
(19) Petty, J. T.; Fan, C.; Story, S. P.; Sengupta, B.; Sartin, M.; Hsiang, J.-C.; Perry, J. W.; Dickson, R. M. *J. Phys. Chem. B* **2011**, *115*, 7996−8003.
(20) Copp, S. M.; Schultz, D.; Swasey, S.; Pavlovich, J.; Debord, M.; Chiu, A.; Olsson, K.; Gwinn, E. *J. Phys. Chem. Lett.* **2014**, *5*, 959−963.
(21) Sengupta, B.; Springer, K.; Buckman, J. G.; Story, S. P.; Abe, O. H.; Hasan, Z. W.; Prudowsky, Z. D.; Rudisill, S. E.; Degtyareva, N. N.; Petty, J. T. *J. Phys. Chem. C* **2009**, *113*, 19518−19524.
(22) Yeh, H. C.; Sharma, J.; Han, J. J.; Martinez, J. S.; Werner, J. H. *Nano Lett.* **2010**, *10*, 3106−3110.
(23) Sharma, J.; Yeh, H. C.; Yoo, H.; Werner, J. H.; Martinez, J. S. *Chem. Commun.* **2011**, *47*, 2294−2296.
(24) Lan, G.-Y.; Chen, W.-Y.; Chang, H.-T. *Biosens. Bioelectron.* **2011**, *26*, 2431−2435.
(25) Li, J.; Zhong, X.; Zhang, H.; Le, X. C.; Zhu, J.-J. *Anal. Chem.* **2012**, *84*, 5170−5174.
(26) Yang, S. W.; Vosch, T. *Anal. Chem.* **2011**, *83*, 6935−6939.
(27) Petty, J. T.; Story, S. P.; Juarez, S.; Votto, S. S.; Herbst, A. G.; Degtyareva, N. N.; Sengupta, B. *Anal. Chem.* **2012**, *84*, 356−364.
(28) Petty, J. T.; Giri, B.; Miller, I. C.; Nicholson, D. A.; Sergev, O. O.; Banks, T. M.; Story, S. P. *Anal. Chem.* **2013**, *85*, 2183−2190.
(29) Shah, P.; Rorvig-Lund, A.; Ben Chaabane, S.; Thulstrup, P. W.; Kjaergaard, H. G.; Fron, E.; Hofkens, J.; Yang, S. W.; Vosch, T. *ACS Nano* **2012**, *6*, 8803−8814.
(30) Tyagi, S.; Kramer, F. R. *Nat. Biotechnol.* **1996**, *14*, 303−308.
(31) Petty, J. T.; Sergev, O. O.; Nicholson, D. A.; Goodwin, P. M.; Giri, B.; McMullan, D. R. *Anal. Chem.* **2013**, *85*, 9868−9876.
(32) Chance, B. *Ann. N.Y. Acad. Sci.* **1998**, *838*, 29−45.
(33) Frangioni, J. V. *Curr. Opin. Chem. Biol.* **2003**, *7*, 626−634.
(34) Petty, J. T.; Sengupta, B.; Story, S. P.; Degtyareva, N. N. *Anal. Chem.* **2011**, *83*, 5957−5964.
(35) Goldberg, R. N.; Kishore, N.; Lennen, R. M. *J. Phys. Chem. Ref. Data* **2002**, *31*, 231−370.
(36) Leroy, J. L.; Gehring, K.; Kettani, A.; Gueron, M. *Biochemistry* **1993**, *32*, 6019−6031.

(37) Doose, S.; Barsch, H.; Sauer, M. *Biophys. J.* **2007**, *93*, 1224−1234.
(38) Petty, J. T.; Fan, C.; Story, S. P.; Sengupta, B.; St. John Iyer, A.; Prudowsky, Z.; Dickson, R. M. *J. Phys. Chem. Lett.* **2010**, *1*, 2524−2529.
(39) Schultz, D.; Gwinn, E. G. *Chem. Commun.* **2012**, *48*, 5748−5750.
(40) Petty, J. T.; Zheng, J.; Hud, N. V.; Dickson, R. M. *J. Am. Chem. Soc.* **2004**, *126*, 5207−5212.
(41) Sengupta, B.; Ritchie, C. M.; Buckman, J. G.; Johnsen, K. R.; Goodwin, P. M.; Petty, J. T. *J. Phys. Chem. C* **2008**, *112*, 18776−18782.
(42) Akers, G. K. In *The Proteins*; Neurath, H., Hill, R. L., Eds.; Academic Press: New York, 1975; Vol. *1*, p 547.
(43) Rivetti, C.; Guthold, M.; Bustamante, C. *J. Mol. Biol.* **1996**, *264*, 919−932.
(44) Huang, C. Y. *Methods Enzymol.* **1982**, *87*, 509−525.
(45) Hill, Z. D.; MacCarthy, P. *J. Chem. Educ.* **1986**, *63*, 162.
(46) Wang, J. C. *Proc. Natl. Acad. Sci. U.S.A.* **1979**, *76*, 200−203.
(47) Pinheiro, A. V.; Han, D.; Shih, W. M.; Yan, H. *Nat. Nanotechnol.* **2011**, *6*, 763−772.
(48) Bertino, M. F.; Sun, Z.-M.; Zhang, R.; Wang, L.-S. *J. Phys. Chem. B* **2006**, *110*, 21416−21418.
(49) Provorse, M. R.; Aikens, C. M. *J. Am. Chem. Soc.* **2010**, *132*, 1302−1310.
(50) Phan, A. T.; Gueron, M.; Leroy, J. L. *Methods Enzymol.* **2001**, *338*, 341−371.
(51) Gwinn, E. G.; O'Neill, P.; Guerrero, A. J.; Bouwmeester, D.; Fygenson, D. K. *Adv. Mater.* **2008**, *20*, 279−283.
(52) Soto-Verdugo, V.; Metiu, H.; Gwinn, E. *J. Chem. Phys.* **2010**, *132*, 195102.
(53) Percivalle, C.; Bartolo, J. F.; Ladame, S. *Org. Biomol. Chem.* **2013**, *11*, 16−26.
(54) Silverman, A. P.; Kool, E. T. *Chem. Rev.* **2006**, *106*, 3775−3789.
(55) Seeman, N. C. *Annu. Rev. Biochem.* **2010**, *79*, 65−87.
(56) Aikens, C. M.; Li, S.; Schatz, G. C. *J. Phys. Chem. C* **2008**, *112*, 11272−11279.
(57) Guidez, E. B.; Aikens, C. M. *Nanoscale* **2012**, *4*, 4190−4198.
(58) Brown, D. M.; Gray, D. M.; Patrick, M. H.; Ratliff, R. L. *Biochemistry* **1985**, *24*, 1676−1683.
(59) Gueron, M.; Leroy, J. L. *Curr. Opin. Struct. Biol.* **2000**, *10*, 326−331.